Characterization of nano-structured W, Ti, V, and Zr doped carbon films

M. Balden

Max-Planck-Institut für Plasmaphysik, EURATOM Association, 85748 Garching, Germany

Abstract

Bonding structure of carbon and metal as well as nanostructural changes of metal-doped amorphous carbon films (a-C:Me) were investigated depending on metal type (W, Ti, V, Zr), concentration (<25 at%) and annealing temperature (<1300 K, except W: <2800 K). Pure C films exhibit ~2 nm distorted aromatic and graphene-like regions. Both increase in size with annealing. After deposition the metals have carbide-like bonding and are mainly distributed atomically disperse in an amorphous environment. Annealing leads to formation of carbide crystallites (TiC, VC, ZrC, WC, W_2C, WC_{1-x}) of several nm. The VC particles reach the largest size up to 1300 K. All metal dopings reduce the erosion rate against oxidation (expect V) and hydrogen impact.

Keywords: Metal-containing carbon films; a-C; carbon bonding; carbide formation; oxidation; plasma-facing material

*Corresponding author e-mail: Martin.Balden@ipp.mpg.de

*Corresponding author address: Boltzmannstrasse 2, 85748 Garching, Germany

*Corresponding author phone: + 49 89 3299 1866

*Corresponding author fax: + 49 89 3299 1212

1. Introduction

Metal-containing carbon films (a-C:Me, a-C:H:Me) are intensively studies regarding to various possible applications [1-21]. Their outstanding tribological and mechanical properties, especially wear resistance and hardness, pushed their research forward [2-11]. In recent years also their optical and electrical properties as well as their biocompatibility got more and more attention [11-21]. Detailed knowledge of the formation of their nanostructure is necessary for designing their properties for the different applications.

In the field of nuclear fusion, such metal-containing films appear as by-product due to the used mixture of plasma-facing materials (PFM) in existing and future fusion plasma devices [22-27]. The PFMs are eroded by intensive energetic particle and high power loads. The nowadays used and proposed PFMs for future devices are tungsten, carbon and beryllium.

The use of carbon as PFM has been resulted to some breakthroughs in fusion plasma physics [28]. But its strong chemical reactivity with hydrogen leads to high erosion yields under hydrogen impact and to high hydrogen amounts in deposited films [29,30]. This leads to the safety issue of tritium inventory in future fusion plasma devices using the mixture of deuterium and tritium – the fuel for a fusion power plant. Therefore, it is required that the possibly eroded amount of carbon is minimized, e.g., by limiting the use of carbon or by reducing the erosion yield by doping graphite with metal carbides, as it is shown for TiC, ZrC or VC [31,32]. For trustable assessments of the tritium inventory, basic knowledge about the hydrogen retention behaviour in the used materials as well as

in the deposited films is needed. To manage the tritium inventory, removal techniques of tritium or even of the complete films, e.g., by oxidation, are considered [29,33,34].

In order to obtain basic knowledge about the mechanism of the reduced chemical erosion of doped graphite as well as the re-erosion of deposited mixed films in fusion plasma devices, magnetron sputtered a-C:Me films (Me: W, Ti, V, Zr) with metal concentration between 0 and 25 at% are investigated in detail as a model system over the last year leading to several publications [35-51].

This paper reviews and summarises the results of the detailed characterisation regarding the distribution of the metal in the a-C:Me films, their clustering and phase formation due to annealing as well as the bonding situation in the carbon matrix. Furthermore, fusion relevant properties are studied, e.g., erosion and hydrogen retention in the films by hydrogen impact as well as their oxidation behaviour.

2. Film production and annealing

2.1. Film production

The studied a-C and a-C:Me films were produced by non-reactive multi source magnetron sputter deposition. Argon was used as sputtering gas with a working pressure of ~0.5 Pa resulting from controlled Ar influx of 20 sccm (base pressure 2-5x10^{-5} Pa). A RF power of 500 W was applied to the graphite cathode, while the metal cathode was operated in DC mode with different powers to achieve a metal concentration ranging from 0 to 25 at% metal in the films. Deposition rates of about 0.05 nm/s were reached.

The specimens were not intentionally heated. Their temperature did not exceed 350 K during deposition. The specimen holder rotated with 10 rounds/minute. All 10 – 30 specimens of each deposition run were placed on a circle to ensure equality of the deposited films. The specimens were cleaned by Ar plasma for a few minutes (100 W, 550-600 V). No bias was applied during film deposition. More details about the film deposition can be found in [38]. More then 100 different deposition runs were performed over the years.

Polished graphite plates and Si wafer pieces were usually used as substrate. For some special experiments glass, sapphire and SiC were required as substrate. All substrates were cleaned in ultrasonic bath of isopropanol. The films were deposited as single layer or as triple layers, sandwiching the metal-containing layer between two pure a-C layers in order to reduce surface and substrate effects.

2.2. Annealing of films

The annealing in vacuum up to 1300 K was performed in different furnaces with a base pressure better than $5x10^{-4}$ Pa. Annealing durations between 0.25 and 2 h were applied.

The annealing above 1300 K up to 2800 K was performed in a furnace with graphite interior under He atmosphere. The annealing temperature was hold for 1 h. Only W-doped specimens were annealed above 1300 K until now.

For the oxidation experiments, the specimens were heated in air to 550, 600 and 650 K. Various oxidation durations between 0.25 h and 48 h were applied to the different

specimens. For mass loss time series, the samples were removed from the furnace and cooled down to room temperature.

3. Applied characterisation techniques

3.1. Ion beam analysis: RBS and NRA

Rutherford backscattering spectrometry (RBS) measurements were performed at the tandem accelerator (High Voltage) facility, IPP, Garching. For depth resolved composition determination, usually 4 MeV ^{4}He backscattered by 165° were used [38,39]. Lateral homogeneity was controlled by analysing several spots of 1 mm^2 size on several specimens of the same deposition run. For better depth resolution just beneath the surface, lower energies down to 500 keV were used. For determination of total carbon loss, also 1.5 MeV protons were used. The deuterium retention was measured with a 800 keV ^{3}He beam performing nuclear reaction analysis (NRA) [49].

3.2. X-ray diffraction: XRD

Crystallographic phases and crystallite sizes were determined by XRD with Cu Kα radiation. A parabolic multilayer mirror (W/Si) was used on the primary side to achieve a parallel beam. Most diffractograms were recorded at a gracing angle of 1° to 5° [44,45]. Applying the Scherer formula after adequate peak deconvolution and fitting leads to the mean crystallite sizes [52].

3.3. Microscopy

The surface morphology of the film was examined with scanning electron microscopy (SEM) and atomic force microscopy (AFM) in contact or non-contact mode [39,43,45,46]. In order to investigate the build-up of the films, cross-sections and thin lamellas were prepared by simple breaking of the specimen or by focused ion beam (FIB) cross-sectioning. They were analysed with SEM as well as with conventional and scanning transmission electron microscopy (TEM, STEM) [45,51]. In addition, nano diffraction was performed on selected specimens in STEM [52].

3.4. X-ray absorption fine structure measurements: XAFS

In order to get information about the local surrounding and order of the metal atoms and their bonding in the films, XAFS measurements at the K absorption edges of Ti, V, and Zr and the L1 and L3 edge of W were performed at Hasylab (Hamburg) on beamline C and at the ESRF (Grenoble) on beamline ID26 [39,40,44,45]. To obtain the sp^2 carbon bonding content, the near edge structure of the carbon edge was investigated at the SRS Daresbury Laboratory on beamline 1.1 [45,47].

3.5. Raman spectroscopy

The sp^2 carbon bonds were investigated by Raman spectroscopy. The spectra were recorded between 900 – 1900 cm^{-1} with a Renishaw 1000 microscope using an argon ion laser at 514.5 nm. The resulting peak structures – known as *D* and *G* peak [53] – were fitted by an asymmetrical line shape of Breit-Wigner-Fano type [45,48]. The

interpretation of the *D* to *G* intensity ratio as well as the peak width and shift is accordingly to [53].

3.6. Deuterium exposure

The films were exposed to energetic hydrogen by a mass-separated, mono-energetic ion beam and by RF low temperature plasma [35,36,43]. The hydrogen isotope deuterium (D) was always used. The total erosion yield was determined by weight loss and by RBS measurements [37,41,42]. The time dependence of the yield was obtained from mass spectrometer data (ion source) and optical emission spectroscopy (RF plasma). In addition, the mass spectrometer data gave an indication for the chemical erosion of the carbon by deuterium, i.e., the formation of methane (CD_4) [42].

Further more, the retained deuterium in the films was determined with NRA in dependence on doping, pre-annealing and implantation temperature, and D fluence [49].

4. Characterisation results

4.1. Composition, thickness, morphology, adhesion and hardness

Metal concentrations of films in the range of 0-25 at% are deposited. A slight increase of concentration with distance from substrate interface is observed [38]. The deposition is laterally homogenous, less than 5% variation. As impurities O and Ar are always present. The O concentration is normally below 1 at%, while the Ar concentration of around 2

at% is slightly varied by the dopant. The dopant cross-contamination from previous deposition is below 0.01 at% at the interface substrate to coating.

The thickness of all films is between 0.1 to 4 μm, but the most films are about 1 μm thick. The thickness is obtained by profilometry on an artificial film edge of one specimen per deposition run, by microscopy on cross-sections, by weighing the specimens before and after film deposition and by RBS. The combination reveals reasonable density of around 10^{23} at/m^3 [38].

The appearance of the surface topography of all films after deposition is very similar. Figure 1(a) shows the surface of a pure carbon film. Small, about 10 nm large structures are dominating the surface, while larger nearly circular structures (several 100 nm) are present. On Si wafer substrate, the latter ones cover less than 1% of the surface, but their density strongly increases on other substrate, i.e. graphite. In cross-sections they exhibit their columnar structure, Fig. 1(b). The roughness obtained from AFM for all initial films on Si is similar, too [39].

Simple scratch test with a needle exhibits good adhesion and high hardness of the films. No aging is observed for the most films, even after >5 years storage at air. For some films, the hardness is determined by nano indentation to be ~14 GPa, while their elastic modulus is ~200 GPa [39]. Note that hydrogen exposure (see 4.4) could soften the films drastically so that the contact mode in AFM fails to image the surface [43].

4.2. Bonding structure of carbon

In the as-deposited a-C films, a sp^2 fraction of the carbon bonds of ~80% is determined by NEXAFS [45,47]. Annealing to 1300 K increases this fraction to ~95%. The analysis of the Raman spectra regarding the *D* to *G* peak intensity ratio indicates that small aromatic areas are present in the as-deposited films. Their size increases with annealing [48]. In addition, diffraction from graphene-like areas is observed with XRD (graphene peaks). These areas increase also in size with annealing. It is proposed that these graphene-like areas of 2-3 nm size are embedded in a matrix dominated by distorted aromatic ring systems [45,48].

The effect of metal doping on the size of the distorted aromatic ring systems is show on the example of zirconium in Fig. 2. The addition of dopant increases their size, even above the level of annealed a-C films. This effect is present for all four investigated dopants, strongest for Zr and Ti, and less for V and W [45,48]. It can be assumed from existing data that the concentration effect has a maximum around 20 at% metal. Annealing diminishes this effect for all doped films. So, the carbon bonding structure in the matrix of annealed a-C:Me films is equal, independent of the metal concentration and type.

4.3. Structure of metal

From XAFS investigations, it can be concluded for all as-deposited doped films that the metal atoms are distributed atomically disperse in an amorphous, disordered carbon surrounding. The metal atoms are in a carbide-like bonding configuration [45].

Annealing leads to clustering and formation of carbide crystallites of several nm in size. Already 900 K is sufficient to arrange the majority of the metal atoms in carbide structure up to the 2nd next neighbours as deduced from XAFS. Observed by XRD, the achievable size of crystallites by annealing to 1300 K is largest for V (Fig. 3: ~10 nm), followed by Ti, Zr, and then W. The dopant concentration influences slightly the size. Comparing TEM data with XRD reveals that the crystallite size exhibits a broad distribution of VC, TiC, and ZrC.

Because for W-doped C films XRD fails to attribute the phase of the dopant up to 1300 K, higher annealing temperatures and STEM with nano diffraction are applied. Three different thermo dynamical stabile tungsten carbide phases [55] are found by XRD: WC, W_2C, and WC_{1-x} [51]. The appearance of phase depends on dopant concentration and annealing temperature, e.g., the 9 at% W-doped film annealed at 2200 K is dominated by WC_{1-x} with an addition of W_2C, while the 18 at% W-doped film annealed at 1450 K and 2200 K shows a mixture of WC and W_2C [51]. The occurrence of the phases is confirmed by nano diffraction in STEM. In addition, it is shown in STEM with nano diffraction that 2-3 nm large carbide crystallites (WC_{1-x}, W_2C) are already formed on 9.5 at% W film at 1300 K. Even if the XRD features on the as-deposited W-doped films are already intense, no indication of crystallites could be observed in STEM [51].

Higher annealing temperature (above 1300 K) allows to obtain even larger crystallite sizes. E.g, for a 9 at% W-doped film after 2800 K annealing, a broad distribution of crystallite sizes between ~10 nm and several 100 nm is observed (Fig. 4).

Concluding, annealing leads to nm-sized carbide crystallites embedded in a matrix dominated by distorted aromatic regions with some graphene-like areas.

4.4. Oxidation behaviour

By exposing the specimens to air at 550 – 650 K and measuring their weight change as well as their compositional change (RBS), oxidation rates are evaluated [46]. The uptake of oxygen and the formation of an oxide layer covering the surface are observed by RBS. Figure 5 shows the oxidation rate gained by weight loss for as-deposited 2 and 9.5 at% W-doped films in comparison to pure a-C films and the range of published rates for various graphite grades, from which some are doped. The carbon removal rate for the 2 and 9.5 at% W-doped films is reduced by one and two orders of magnitude, respectively. Tungsten exhibits the highest reduction, follow by Ti and Zr. Vanadium as oxide promotes the carbon oxidation, as expected from its known catalytic behaviour in the oxidation process [56].

The thermal pre-treatment of films, e.g., formation of carbides at 1300 K, could affect the oxidation behaviour of the doped carbon films. Future investigations should be addressed to it.

4.5. Erosion yield and D retention by D impact

The erosion behaviour of metal containing carbon films by hydrogen impact is of vital interest for fusion research [35-37,42-45,50]. Figure 6(a) shows the CD_4 production of pure and 6 at% W-doped carbon films for 30 eV D impact. The methane production is

only an indicator for the chemical erosion of C by D. A drastic change of the temperature dependence of the CD_4 production compared to the pure C film is obvious. This change points to the strong effect of metal doping on the chemical erosion of the carbon from the films. The reduction of the total erosion yield determined by RBS is even stronger, especially at 300 K (Fig. 6(b)). For all four dopants, a similar reduction potential is observed [37,42-44].

In contrast to the erosion, D retention does not show a strong influence by doping. It is only slightly reduced, e.g., the D retention decreases from 10^{21} D/m^2 by maximal about 50% by doping at a D fluence of 10^{24} D/m^2 [49]. This reduction depends on the W concentration and saturates at about 7 at% W to these 50%. The retention behaviour is better described by the exponent of power law dependence of retention on fluence. For pure carbon films an exponent of slightly above 0.1 is found, which reduces to below 0.05 for the 7 at% and higher W-doped films [49].

5. Summary

Magnetron sputter deposited metal-containing carbon films are intensively characterized and their thermal behaviour up to 1300 K for Ti, V and Zr and up to 2800 K for W is investigated. Films with metal concentrations of up to 25 at% and around 1μm thickness were deposited without bias at about room temperature. For these films, the following picture can be drawn:

(i) Pure C films exhibit ~2 nm distorted aromatic and graphene-like regions, which both increase in size with annealing. The implementation of metals in the carbon films

increases the size of the distorted aromatic regions in the carbon matrix. The achieved size depends on metal concentration with a maximum around 20 at%. The difference by doping of the carbon matrix vanishes after annealing at 1300 K.

(ii) Already after deposition, the metals are in carbide-like bonding environment without forming crystallites. They are mainly distributed atomically disperse in an amorphous carbon environment. Due to annealing up to 1300 K carbide crystallites (TiC, VC, ZrC, WC, W_2C, WC_{1-x}) of several nm are formed, which are the largest for VC at 1300 K (several tens of nm). Higher annealing above 1300 K of the W-doped films leads to even larger crystallites. By choosing the metal concentration as well as the annealing temperature and duration the crystallite size can be adjusted, but the crystallite size distribution is quite broad or even bimodal.

(iii) The oxidation rate of the W, Ti Zr doped films is strongly reduced compared to the pure C films, while V doping promotes the oxidation of the carbon. The erosion yield against hydrogen impact is strongly reduced for all four dopants. Reduction by one order of magnitude is easily achieved. The retention of hydrogen after hydrogen impact is slightly decreased by doping with W (others dopants not studied jet).

Acknowledgement

I would like to thank many colleagues and co-operation partners for participating over the years in this characterisation project: C. Adelhelm, B.T. Cieciwa, E. Cochrin, S. Denis, A. Dorner, B. Dubiel, M. Fußeder, A. Herrmann, S. Jong, E. de Juan Pardo, F. Koch, T. Köck, F. Kost, S. Lindig, J. Jaimerena-Muga, G. Matern, T. Plocinski, I.

Quintana, M. Rasinski, M. Rinke, J. Roth, P.A. Sauter, K.I. Schiffmann, I. Sergues-Guridi, M. Sikora, L. Sinclair, P. Starke, M. Stüber, A. Weghorn, and E. Welter.

References

[1] A. Schüler, D. Babonneau, M. Balden, Solid State Sci. 11 (2009) 1737.

[2] H. Dimigen, H. Hübsch, R. Memming, Appl. Phys. Lett. 50 (1987) 1056.

[3] A.A. Voevodin, S.V. Prasad, J.S. Zabinski, J. Appl. Phys. 82 (1997) 855.

[4] W. J. Meng and B.A. Gillispie, J. Appl. Phys. 84 (1998) 4314.

[5] S.J. Park, K.-R. Lee, D.-H. Ko, K.Y. Eun, Diamond Relat. Mater. 11 (2002) 1747.

[6] D. Nilsson, F. Svahn, U. Wiklund, S. Hogmark, Wear 254 (2003) 1084.

[7] K.I. Schiffman, Surf. Coat. Technol. 177-178 (2004) 453.

[8] Y.T. Pei, D. Galvan, J.Th.M. De Hosson, J. Vac. Sci. Technol. A 24 (2006) 1448.

[9] A.Y. Wang, K.-R. Lee, J.-P. Ahn, J.H. Han, Carbon 44 (2006) 1826.

[10] J.C. Sanchez-Lopez, D. Martínez-Martínez, M.D. Abad, A. Fernández, Surf. Coat. Technol. 204 (2009) 947.

[11] T. Polcar, T. Vitu, L. Cvrcek, R. Novak, J. Vyskocil, A. Cavaleir, Solid State Sci. 11 (2009) 1757.

[12] C. Benndorf, M. Grischke, H. Koeberle, R. Memming, A. Brauer, F. Thieme, Surf. Coat. Technol. 36 (1988) 171.

[13] C. Corbella, G. Oncins, M.A. Gomez, M.C. Polo, E. Pascual, J. Garcia-Cespedes, J.L. Andujar, E. Bertran, Diamond Relat. Mater. 14 (2005) 1103.

[14] E. Lewin, O. Wilhelmsson, U. Jansson, J. Appl. Phys. 100 (2006) 054303.

[15] J.L. Endrino, D. Horwat, R. Gago, J. Andersson, Y.S. Liu, J. Guo, A. Anders, Solid State Sci. 11 (2009) 1742.

[16] R.G. Agostino, T. Caruso, G. Chiarello, A. Cupolillo, D. Pacile, R. Filosa, V. Formoso, E. Colavita, L. Papagno, C. Ducati, E. Barborini, C. Lenardi, G. Bongiorno, P. Piseri, P. Milani, Phys. Rev. B 68 (2003) 035413.

[17] R. Koppert, D. Goettel, O. Freitag-Weber, G. Schultes, Solid State Sci. 11 (2009) 1797.

[18] R. Hauert, Diamond Relat. Mater. 12 (2003) 583.

[19] M.L. Morrison, R.A. Buchanan, P.K. Liaw, C.J. Berry, R.L. Brigmon, L. Riester, H. Abernathy, C. Jin, R.J. Narayan, Diamond Relat. Mater. 15 (2006) 138.

[20] M. Andara, A. Agarwal, D. Scholvin, R.A. Gerhardt, A. Doraiswamy, C. Jin, R.J. Narayan, C.-C. Shih, C.-M. Shih, S.-J. Lin, Y.-Y. Su, Diamond Relat. Mater.15 (2006) 1941.

[21] F. Schwarz, G. Thorwarth, B. Stritzker, Solid State Sci. 11 (2009) 1819.

[22] R. Behrisch, M. Mayer, C. Garcia-Rosales, J. Nucl. Mater. 233-237 (1996) 673.

[23] M. Mayer, R. Behrisch, P. Andrew, J.P. Coad, A.T. Peacock, Phys. Scr. T 81 (1999) 13.

[24] D. Hildebrandt, P. Wienhold, W. Schnieder, J. Nucl. Mater. 290-293 (2001) 89.

[25] H. Kleykamp, J. Nucl. Mater. 301 (2002) 233.

[26] J. Likonen, E. Vainonen-Ahlgren, L. Khriachtchev, J.P. Coad, M. Rubel, T. Renvall, K. Arstila, D.E. Hole, Contributors to the EFDA-JET Work-programme, J. Nucl. Mater. 377 (2008) 486.

[27] M. Psoda, M. Rubel, G. Sergienko, P. Sundelin, A. Pospieszczyk, J. Nucl. Mater. 386-388 (2009) 740.

[28] J. Winter, J. Nucl. Mater. 145-147 (1987) 131.

[29] G. Federici, C.H. Skinner, J.N. Brooks, J.P. Coad, C. Grisolia, A.A. Haasz, A. Hassanein, V. Philipps, C.S. Pitcher, J. Roth, W.R. Wampler, D.G. Whyte, Nucl. Fusion 41 (2001) 1967.

[30] J. Roth, E. Tsitrone, A. Loarte, Th. Loarer , G. Counsell, R. Neu, V. Philipps, S. Brezinsek, M. Lehnen, P. Coad, Ch. Grisolia, K. Schmid, K. Krieger, A. Kallenbach, B. Lipschultz, R. Doerner, R. Causey V. Alimov, W. Shu, O. Ogorodnikova, A. Kirschner, G. Federici, A. Kukushkin, EFDA PWI Task Force, ITER PWI Team, Fusion for Energy, ITPA SOL/DIV, J. Nucl. Mater. 390-391 (2009) 1.

[31] C. Garcia-Rosales and M. Balden, J. Nucl. Mater. 290-293 (2001) 173.

[32] C. Garcia-Rosales, I. López-Galilea, N. Ordás, C. Adelhelm, M. Balden, G. Pintsuk, M. Grattarola, C. Gualco, J. Nucl. Mater. 386-388 (2009) 801.

[33] S. Alberici, J.P. Coad, H.-K. Hinssen, R. Moormann, P. Wienhold, C.H. Wu, J. Nucl. Mater. 258-263 (1998) 764.

[34] C.H. Skinner, A.A. Haasz, V.Kh. Alimov, N. Bekris, R.A. Causey, R.E.H. Clark, J.P. Coad, J.W. Davis, R.P. Doerner, M. Mayer, A. Pisarev, J. Roth, T. Tanabe, Fusion Sci. Technol. 54 (2008) 891.

[35] E. de Juan Pardo, M. Balden, B. Cieciwa, C. Garcia-Rosales, J. Roth, Phys.. Scr. T111 (2004) 62.

[36] E. de Juan Pardo, Ph.D.Thesis, ”Characterisation and Mitigation of Chemical Erosion of Doped Carbon Materials”, Report IPP 17/3, Max-Planck-Institut für Plasmaphysik (2004).

[37] M. Balden, E. de Juan Pardo, I. Quintana, B. Cieciwa, J. Roth, J. Nucl. Mater. 337-339 (2005) 980.

[38] M. Balden, B.T. Cieciwa, I. Quintana, E. de Juan Pardo, F. Koch, M. Sikora, B. Dubiel, Surf. Coat. Technol. 200 (2005) 413.

[39] M. Balden, C. Adelhelm, T. Köck, A. Herrmann, J. Jaimerena-Muga, Rev. Adv. Mater. Sci. 15 (2007) 95.

[40] C. Adelhelm, M. Balden, M. Sikora, Mater. Sci. and Eng. C 27 (2007) 1423.

[41] M. Balden, C. Adelhelm, E. de Juan Pardo, J. Roth, J. Nucl. Mater. 363-365 (2007) 1173.

[42] M. Balden and C Adelhelm, Phys. Sci. T128 (2007) 121.

[43] P. Starke, C. Adelhelm, M. Balden, Contrib. Plasma Phys. 47 (2007) 530.

[44] M. Balden, C. Adelhelm, M. Sikora, J. Nucl. Mater. 367-370 (2007) 1458.

[45] C. Adelhelm, Ph.D Thesis, ”Structure and Erosion Behavior of Metal-doped Carbon Films”, Report IPP 17/11, Max-Planck-Institut für Plasmaphysik (2008).

[46] I. Segues Guridi, Thesis, ”Oxidation behavior of metal doped carbon films”, Universidad de Navarra, San Sebastian (2008).

[47] C. Adelhelm M Balden, F Kost, A Herrmann, S Lindig, Journal of Physics: Conference Series 100 (2008) 062033.

[48] C. Adelhelm, M. Balden, M. Rinke, M. Stueber, J. Appl. Phys. 105 (2009) 033522.

[49] P.A. Sauter and M. Balden, Phys. Sci. T138 (2009) 014044.

[50] P.A. Sauter and M. Balden, ”Temperature dependence of the erosion behaviour of deuterium beam exposed tungsten-doped carbon films (a-C:W)”, J. Nucl. Mater. in press DOI information: 10.1016/j.jnucmat.2010.08.021.

[51] P.A. Sauter, M. Balden, S. Jong, C. Adelhelm, S. Lindig, M. Rasinski, T. Plocinski, Thin Solid Films, “Carbide formation in tungsten-containing amorphous carbon films by annealing”, submit to Thin Solid Films (Proceeding of this symposium).

[52] M. Birkholz, *Thin Film Analysis by X-Ray Scattering*, Wiley-VCH, Weinheim, 2006

[53] A.C. Ferrari and J. Robertson, Phys. Rev B 61 (2000) 14095.

[54] M. Balden, K.U. Klages, W. Jacob, J. Roth, J. Nucl. Mater. 341 (2005) 31.

[55] A.S. Kurlov and A.I. Gusev, Inorganic Materials 42 (2006) 121.

[56] J.P.A. Neeft, M. Makkee, J.A. Moulijn, Chem. Eng. J. 64 (1996) 295.

Figure captions

Fig. 1*: a) Surface morphology of an as-deposited pure carbon film on Si; b) Cross-section through an as-deposited triple layer structure with a 13 at% W layer sandwiched between two pure carbon layers on graphite.*

Fig. 2*: D to G peak intensity ratio of the Raman spectra from carbon films doped with different Zr concentration (data from [48]): as-deposited (open symbols) and after 1300 K annealing (filled symbols). Size evaluation is adopted from [54].*

Fig. 3*: Crystallite size determined with XRD of V-doped carbon films in dependence of annealing temperature and V concentration (data from [45]).*

Fig. 4: *Cross-section of a 9 at% W-doped C film after annealing to 2800 K (lower part: graphite substrate).*

Fig. 5*: Oxidation rates gained from mass loss of not-preannealed undoped and W-doped carbon films (data from [46]). Dashed lines: range of oxidation rates of different graphite grades, partly doped [55].*

Fig. 6*: a) Methane production yield of pure and W-doped carbon films for 30 eV D impact versus specimen temperature. The CD_4 production yields are normalized to total erosion yield at 1000 eV D impact of pyrolytic graphite. b) Comparison of the total erosion obtained by RBS and of the CD_4 production yield for 30 eV D impact on pure*

and 3 at% W-doped film at 300 and 620 K (data from [37,42]).

Figure

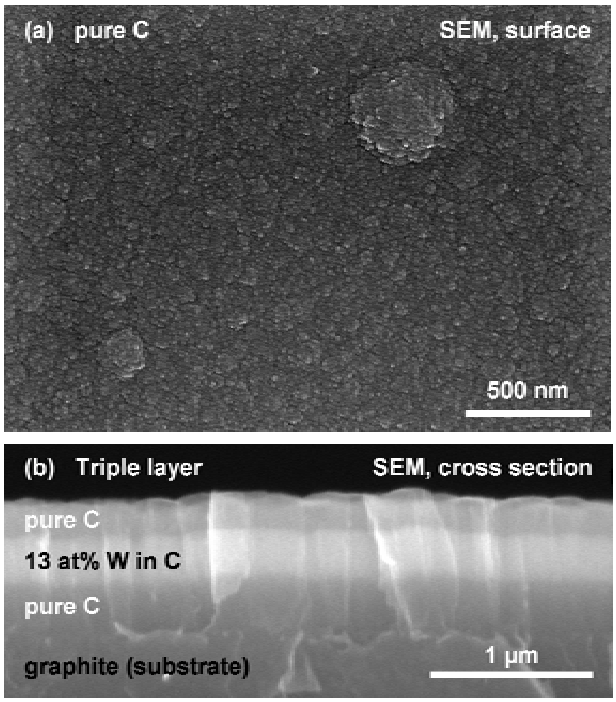

Fig. 1:

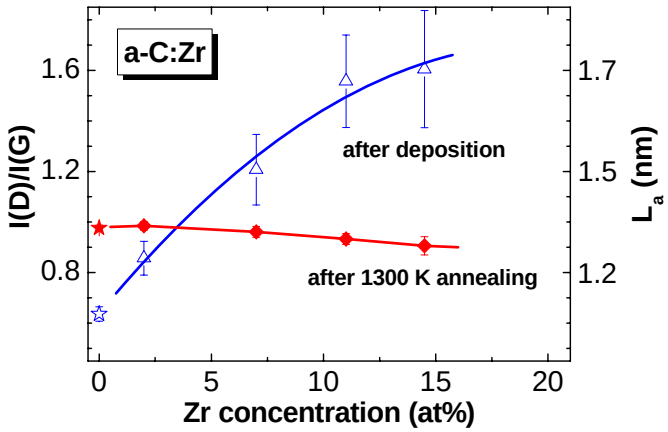

Fig. 2:

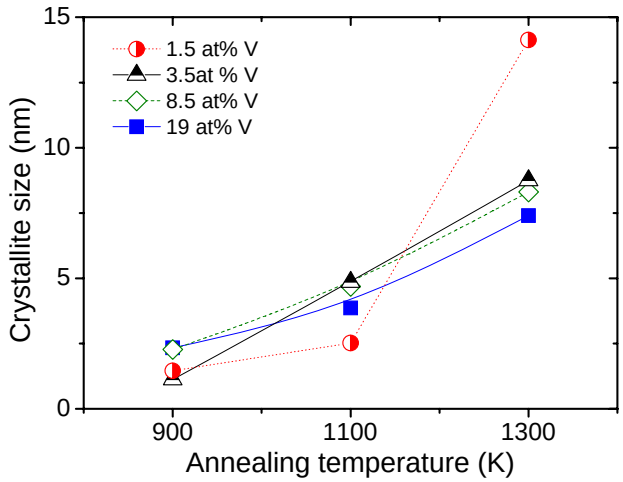
15
10
5
0
Crystallite size (nm)
1.5 at% V
3.5at % V
8.5 at% V
19 at% V
900
1100
1300
Annealing temperature (K)

***Fig. 3*:.**

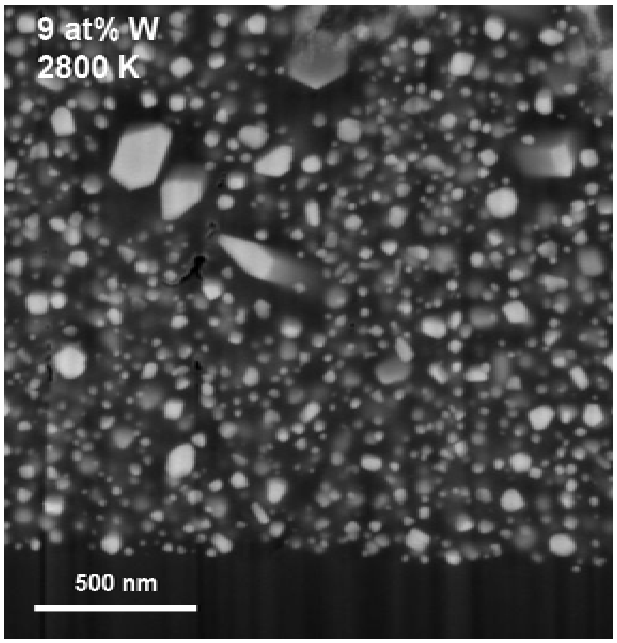
9 at% W
2800 K
500 nm

Fig. 4:

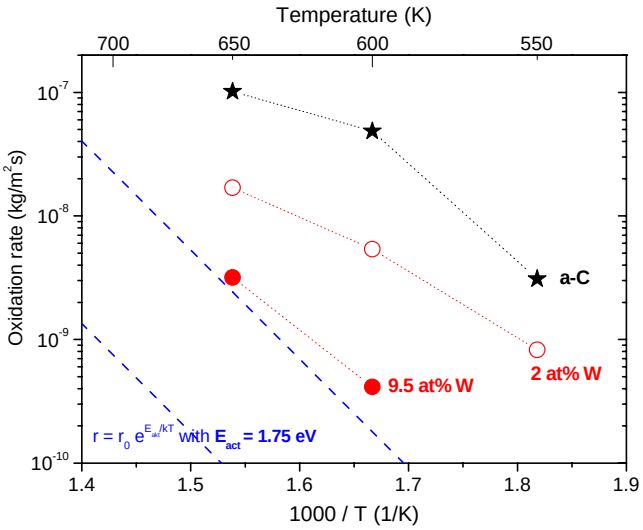
Temperature (K)
700
650
600
550
Oxidation rate (kg/m²s)
10⁻⁷
10⁻⁸
10⁻⁹
10⁻¹⁰
a-C
9.5 at% W
2 at% W
r = r0 e^(Eact/kT) with Eact = 1.75 eV
1.4
1.5
1.6
1.7
1.8
1.9
1000 / T (1/K)

Fig. 5:

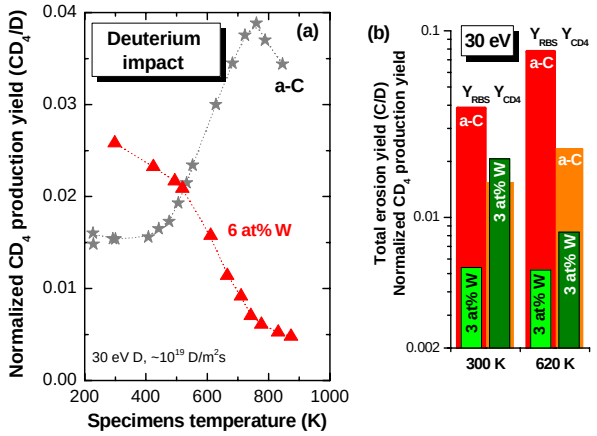
Deuterium impact
(a)
a-C
6 at% W
30 eV D, ~10¹⁹ D/m²s
Normalized CD4 production yield (CD4/D)
0.04
0.03
0.02
0.01
0.00
200
400
600
800
1000
Specimens temperature (K)
(b)
30 eV
Y_RBS Y_CD4
a-C
3 at% W
300 K
620 K
Total erosion yield (C/D)
Normalized CD4 production yield
0.1
0.01
0.002

Fig. 6: